# Pore-scale dynamics of salt precipitation in drying porous media

Mansoureh Norouzi Rad,[1] Nima Shokri,[1,*] and Muhammad Sahimi[2]
[1]*School of Chemical Engineering and Analytical Science, University of Manchester, Manchester M13 9PL, United Kingdom*
[2]*Mork Family Department of Chemical Engineering and Materials Science, University of Southern California, Los Angeles, California 90089-1211, USA*
(Received 3 December 2012; published 9 September 2013)

We study the pore-scale dynamics of salt precipitation in three-dimensional drying porous media, utilizing high resolution x-ray microtomography and scanning electron microscopy. Our results illustrate that the salt precipitation patterns in drying porous media are nonuniform, manifesting the influence of the spatial distribution of pore sizes on the dynamics of salt crystallization and formation of discrete efflorescence. Results reveal that during stage-1 evaporation from saline porous media, the salt precipitation rate initially increases which is followed by a constant precipitation rate. This non-linear behaviour is attributed to the preferential liquid vaporization and salt precipitation in finer pores located at the surface of the porous medium contributing in evaporation according to the pore sizes. We also show that, contrary to common practice, the macroscopic convection-diffusion equation *cannot* provide accurate predictions for the dynamics of salt precipitation, at least at the early stages, due to the microscale heterogeneity of evaporation sites at the surface that results in salt precipitation exclusively in the finer pores.

DOI: 10.1103/PhysRevE.88.032404 PACS number(s): 68.08.−p, 47.56.+r, 47.53.+n, 89.75.Fb

## I. INTRODUCTION

Understanding the physics of salt precipitation in porous media is of fundamental importance to many natural and industrial processes, such as preservation of pavement and historical monuments, mineral-fluid interactions, $CO_2$ sequestration in rock, and the evaporation rates from porous media [1,2]. As water evaporates, the salt concentration in the pore space increases continuously until it exceeds the solubility limit, at which time it precipitates. The precipitation pattern modifies the morphology of the pore space and, consequently, influences flow and transport processes in it. Despite their high importance, particularly to the problem of drinking water for the world's rapidly increasing population, direct pore-scale imaging and the study of salt precipitation and crystallization patterns in three-dimensional (3D) drying porous media are very rare, largely due to the imaging complexity of the dynamics of salt precipitation. Therefore, most of the previous studies were focused on the description of salt deposition patterns at the macroscale and were restricted mostly to two-dimensional (2D) imaging of evaporating surfaces [2,3].

We have employed x-ray microtomography to study the key effects of the pore sizes and the initial salt concentration on dynamics and patterns of salt precipitation in a drying porous medium. Detailed visualization of salt precipitation enables us to identify unambiguously the mechanism of discrete efflorescence on the evaporation surface as a result of the invasion of large pores by air and the subsequent capillary-induced liquid flow toward the fine pores on the surface, where water evaporation occurs preferentially. We establish that the pore-size heterogeneity at the surface of porous media results in heterogeneous distribution of the vaporization sites on the surface and the preferential efflorescence that occurs exclusively in the fine pores. In addition, we quantify the influence of the initial salt concentration on its deposition rate in 3D drying porous media. Finally, we demonstrate that, contrary to common practice, the observed trends cannot be accurately modeled by the convection-diffusion equation (CDE), at least at the early stages.

## II. EXPERIMENTAL CONSIDERATIONS

The drying experiments were carried out in cylindrical plastic columns, 35 mm in height and 11 mm in diameter, packed with sand grains with particle sizes ranging from 0.17 to 1.0 mm, with an average size of 0.58 mm, saturated with NaCl (reagent grade powder from EMD Chemicals, Inc., New Jersey, USA) solutions of 3.5 M (moles of NaCl/kg of water), 4 M, and 6 M. The drying of the sand columns was visualized by means of a HMXST x-ray microtomography system (at 70 kV and 140 $\mu$Å) with spatial and temporal resolutions of 0.021 mm and 30 min. The duration of each round of the experiments was nearly 24 h.

Each 3D scan included 1500 horizontal cross sections. We used the standard machine learning technique of a support vector machine (SVM) [4] with a quadratic kernel to segment each cross section into solid, liquid, and air. The SVMs were trained using sequential minimal optimization [4] from MATLAB's machine learning package. More details about the method are given elsewhere [4]. To distinguish the precipitated salt from the sand grains, each 2D cross section was compared to its corresponding image obtained at the beginning of the experiment, when there was no solid salt in the sample, with the difference indicating the precipitated salt.

The resulting typical cross sections are illustrated in Figs. 1(a)–1(c). Figure 1(d) shows a typical example of the vertical growth of the precipitated salt above the sand surface. The spectrum of yellow to orange (light to medium gray) indicates the time of the scan such that the closer the color is to yellow (light gray), the later the column was scanned. Using this method, we quantify the dynamics of salt growth above the evaporation surface at various times and locations.

*E-mail address: nima.shokri@manchester.ac.uk

 

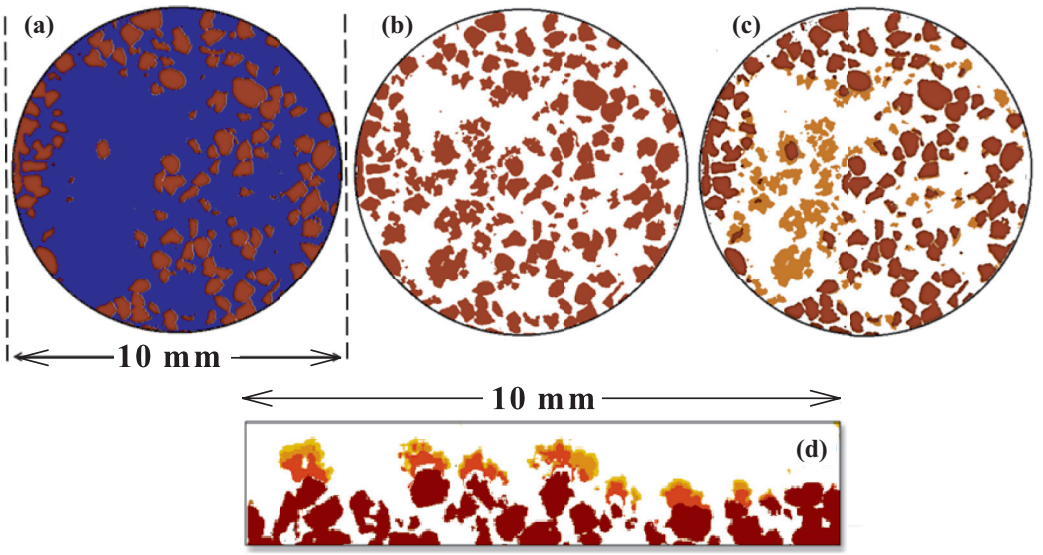


FIG. 1. (Color online) (a) A typical horizontal cross section above the surface, taken at the beginning of the experiment, illustrating the liquid [blue (dark gray)] and solid [brown (medium gray)] phases. (b) The same cross section after 17 h, showing the distribution of the solid [brown (medium gray)] and air (white) phases. (c) The image constructed by comparing the solid phases in (a) and (b) with the difference [orange (light gray)], corresponding to the precipitated salt. (d) A typical vertical close-up of the surface of the sand column saturated with 4 M NaCl solution, constructed by the same method as in (c) and applied to all cross sections. The spectrum of orange to yellow (medium to light gray) indicates the addition of precipitated salt in each scan. Brighter colors indicate longer times.

## III. RESULTS AND DISCUSSIONS

### A. Evaporative water losses

Figure 2 illustrates the cumulative water loss calculated by image analysis. The nearly constant slope of the curves indicates that in all cases the process was in the stage-1 evaporation. The inset in Fig. 2 shows the evolution with time of water saturation at the surface for various initial salt concentrations, confirming the presence of liquid at the surface during the experiments, consistent with the previously reported data [5–7]. The recorded pore-scale images indicate that, at the early stages of the evaporation process, large pores at the surface are invaded preferentially by air, while the fine pores remain saturated due to required higher capillary pressures. These are the characteristics of stage-1 evaporation in which the evaporation rate remains relatively constant and the medium behaves as if it were saturated [5,6]. Results similar to what was reported in Fig. 3 of Shokri *et al.* [5] were obtained in the present study, confirming the presence of continuous liquid pathways between the water-filled fine pores at the surface and the saturated zone at the bottom (which are not repeated here).

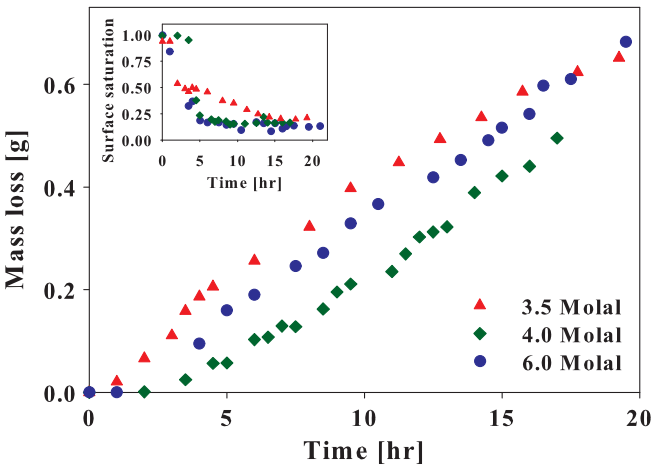


FIG. 2. (Color online) Cumulative mass of liquid water removed by evaporation from the sand columns, initially saturated with various NaCl solutions. The notably lower water evaporation from the 4.0 M solution might be due to the lower atmospheric demand. Although the evaporative demand was nearly constant during each round of the experiment, the relative humidity and temperature inside the x-ray chamber could not be controlled precisely. The inset shows the near surface (the top 0.5 mm) water saturation, confirming the presence of liquid at the surface during the entire course of the experiments.

In the presence of salt, water evaporation from fine pores at the surface results in a continuous increase of salt concentration in the preferential "evaporating spots." When salt concentration reaches the solubility limit, which is 6.12 M for NaCl at 25°C, precipitation takes place, as supersaturation effects are negligible for NaCl [8]. Due to the limited number and discrete nature of the evaporating spots at the surface, salt precipitation occurs at discrete positions that coincide with the locations of the fine pores.

### B. Salt precipitation patterns and dynamics

In Fig. 3 the patterns of the deposited salt at various times from the onset of the experiment are shown, along with the liquid (shown by black) distribution, at the surface of the sand column that was saturated with a 4 M solution. The color scale represents the thickness of the precipitated salt, such that the closer to orange (darker) it is, the larger the thickness is. Figure 3 demonstrates that the nonuniform distribution of the precipitated salt at the surface is influenced by the distribution

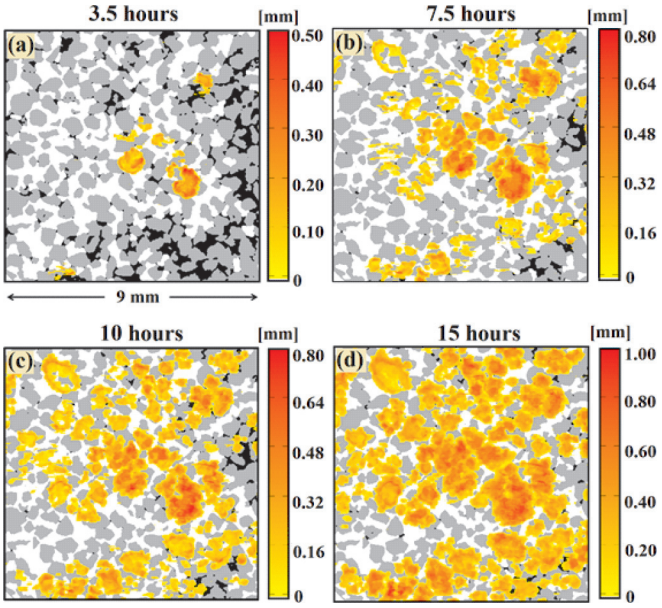


FIG. 3. (Color online) Patterns and distribution of precipitated salt at the surface of the sand column at various times, saturated with the 4 M NaCl solution. The color scale indicates the height of the precipitated salt. Black, gray, and white indicate, respectively, the regions filled with the liquid, sand grains, and the air phase. All other colors correspond to the precipitated salt and the color spectrum indicates the thickness of the precipitated salt such that the closer the color is to orange (darker color), the thicker is the salt crust.

of the pore sizes. Over time, each evaporating spot turned into a precipitation spot, when the salt concentration exceeded the solubility limit. Therefore, the number of precipitation spots increased with time, as indicated by Figs. 3(a)–3(c). When the NaCl concentration exceeded the solubility limit at all the evaporation spots, the number of active pores that contributed to salt precipitation remained constant.

Let us emphasize that what is shown in Fig. 3 is *solely* related to the flow of the liquid toward the evaporating surface, either in the bulk or by film flow, driven by capillary action. A simple analysis clearly demonstrates this. Consider a fully saturated cylindrical pore of radius $r$ with complete evaporation within it. In the absence of convective transport to replenish the evaporating liquid, the volume per unit length occupied by the precipitated salt is $\pi r^2 \gamma/\rho_s$, with $\gamma$ being the solubility and $\rho_s$ being the salt density. Thus, assuming that salt precipitates uniformly on the pore's surface, the available pore volume is $\pi r^2(1-\gamma/\rho_s)$, implying a relative reduction $1-\gamma/\rho_s$ of the pore volume. With $\gamma \approx 0.36$ g/cm$^3$ and $\rho_s \approx 2.165$ g/cm$^3$ for salt density, the fraction is about 0.17. This calculation shows that even after salt precipitation, a part of the pore volume at the surface is still open. Therefore, the evaporating pore could be still hydraulically connected to the wet zone at the bottom via the capillary-induced liquid flow supplying the evaporative demand.

Using the pore-scale data, the salt growth rate at the evaporating surface in each 3D sand column was computed. Figure 4(a) presents the cumulative precipitated salt as a function of the cumulative mass of liquid water lost due to drying. In the case of the sand column initially saturated with a higher salt concentration, more salt has precipitated at the surface for the same mass loss. Figure 4(b) presents the time dependence of the precipitated salt in each sand column indicating that, in the cases of sand columns saturated with 3.5 M and 4 M NaCl solutions, the salt precipitation rate (the *slope* of the line) initially changes with time, followed by a nearly constant value (confirmed by regression analysis). The transition point corresponds to the time at which all evaporation spots serve as the precipitation spots, hence giving rise to a relatively constant precipitation rate. In other words, prior to the transition time, due to water evaporation, salt concentration continuously increases at the surface until it reaches the solubility limit. Therefore, evaporation spots continually turn into precipitation spots at the early stages, resulting in higher precipitation rates, even though the evaporative flux remains nearly constant, as indicated by Fig. 2. After the transition, however, the number of the precipitation spots does not change anymore, and salt continues to deposit on the already existing spots, and hence, the salt precipitation rate remains relatively constant due to the constant drying rate. Interestingly, in the case of the sand

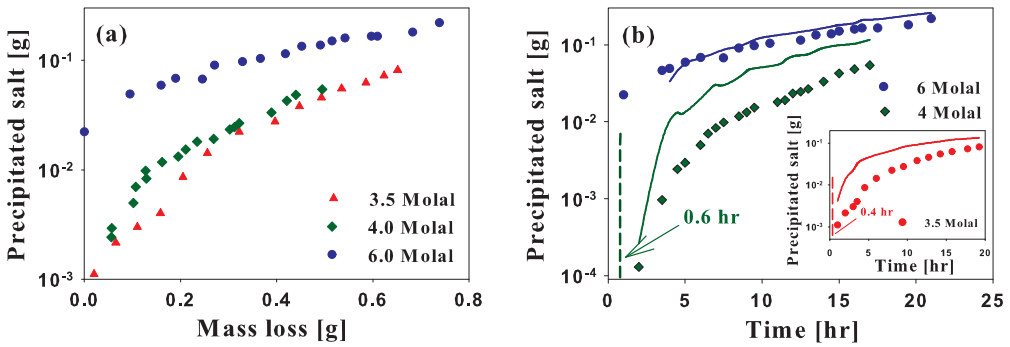


FIG. 4. (Color online) (a) Cumulative precipitated salt as a function of the cumulative mass of liquid water lost by evaporation. The legend indicates the initial salt concentration in each evaporating sand column. (b) Time dependence of the cumulative precipitated salt in each sand column. The precipitation rate (the slope of the curves) changes with time until it becomes nearly constant in the cases of the columns saturated with 3.5 M and 4 M solutions. The transition time to a constant precipitation rate is the time at which all the evaporation spots at the surface turn into precipitation spots. Solid lines correspond to the precipitated salt at the surface over time predicted by convection. The vertical dash lines indicate the onset of NaCl precipitation at the surface predicted by the numerical solution of the CDE which is in a reasonable agreement with the experimental data.

column saturated with a 6 M solution, the salt deposition rate remains nearly constant during the entire course of the experiment because the initial salt concentration is very close to the solubility limit of NaCl, and all the evaporation spots are quickly (within a few minutes) transformed into precipitation spots after the onset of the experiment.

### C. Numerical analysis

During stage-1 evaporation, the ions are transported by convection toward the evaporation surface via the capillary-induced liquid flow. However, diffusion tends to spread the salt uniformly through the entire space. Therefore, the dynamics of the salt distribution is determined by the competition between convective and diffusive fluxes. To quantify the dynamics, the *macroscale* CDE has traditionally been used, but it has never been established that the CDE can actually model the phenomenon quantitatively. Thus, to test this possibility we solved the continuum CDE numerically and estimated the time required to reach the limit of NaCl solubility at the evaporation surface that marks the onset of salt precipitation. The one-dimensional CDE, traditionally used for this purpose, for a porous medium of length $L$ is given by [9,10]

$$\frac{\partial}{\partial t}(\epsilon\rho SC) = \frac{\partial}{\partial z}\left(\rho\epsilon SD\frac{\partial C}{\partial z}\right) - \frac{\partial}{\partial z}(\rho\epsilon SCU)\,, \qquad (1)$$

where $\rho$ is the solution density, $\epsilon$ is the porosity, $S$ is the liquid saturation, $C$ is the salt's mass fraction dissolved in the liquid phase, $D$ is the solute's effective diffusivity, and $U$ is the average liquid velocity. The initial porosity is 0.4, and we neglect its mild changes as salt precipitates. The boundary conditions are that the diffusive and convective fluxes are equal at $z = 0$ and $z = L$, as the ions cannot escape the liquid phase. $D$ was taken to be $10^{-9}$ m$^2$ s$^{-1}$ [4,5,9]. We assume that the liquid saturation is spatially uniform and varies with time as $S = 1 - E/(\rho\epsilon L)t$ [9], where $E$ is the evaporation rate. As the evaporation is slow, the spatial variation of $S$ is very slow and thus is neglected. More details of the numerical simulation of the CDE are given elsewhere [9,10].

As shown in Fig. 4, the CDE predicts 0.4 and 0.6 h as the times required to reach the salt solubility limit at the surface of sand columns saturated with 3.5 M and 4 M NaCl solutions, respectively. Solid lines correspond to the predicted precipitated salt at the surface as a result of convection. As the comparison indicates, the macroscale convective flux cannot by itself describe the dynamics of precipitation at the early and intermediate stages because it cannot account for the pore-scale effect that pores at the surface do not reach the salt solubility limit at the same time (shown in Fig. 3) because they have different sizes and contribute differently to water evaporation. One must carry out pore-scale simulation to account for such an effect. We note that, in the case of the 6 M solution, the macroscale convective flux provides a reasonable estimate of the precipitated salt at the surface because in this case the salt concentration is very close to the solubility limit, and thus, most of the evaporating spots act as the precipitation sites. This means that as water evaporates, the salt transferred to the surface by capillary flow precipitates there, but this is not necessarily the case in the 3.5 and 4 M columns.

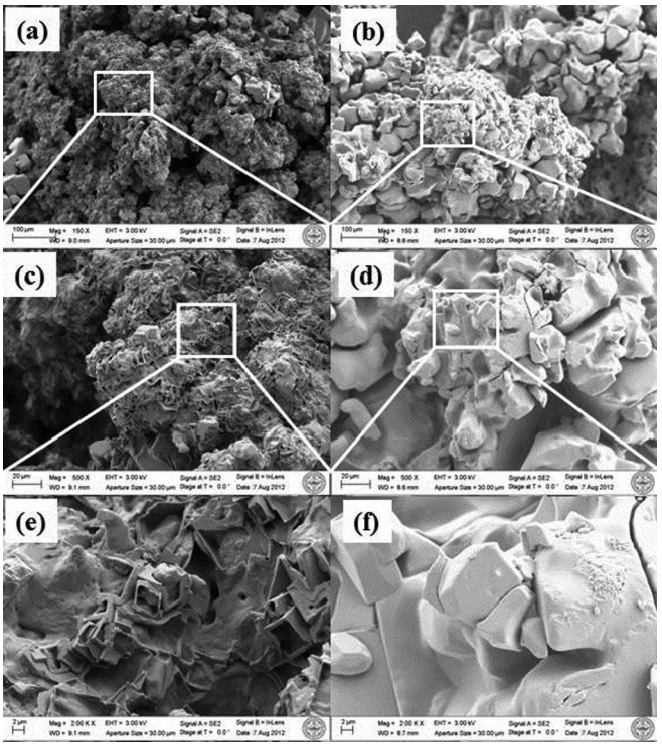


FIG. 5. The SEM images, showing the structure of the precipitated salt at the surface of the sand column, saturated with a 3.5 M NaCl solution after (left) 18 and (right) 168 h with magnification factors of (a) and (b) 150, (c) and (d) 500 and (e) and (f) 2000.

### D. Structural evolution of the precipitated salt

A puzzling question is why during stage-1 evaporation the drying rate remains nearly constant, whereas the surface is covered by the precipitated salt. For example, in the case of the 6 M NaCl solution, the evaporation surface is covered quickly by the precipitated salt, but as illustrated by Fig. 2, the evaporation rate remains relatively constant. This phenomenon may be explained by considering two main factors, namely, the preferential locations of salt precipitation and the structure of the precipitated salt. The initiation and growth of the salt crystals occur on the grains, not inside the pores, as illustrated in Fig. 1(d), because the energy of heterogeneous nucleation (the formation of the crystal nuclei on preferential nucleation sites, such as solid particles or the surface) is lower than that of the homogeneous process of nucleation in the supersaturated liquid under the conditions of our experiment [11].

The second factor can be related to the structure of the precipitated salt. We used scanning electron microscopy (SEM) to image the evolution of the precipitated salt structure at various times and length scales, down to a few hundred nanometers. The SEM images indicate that the growing precipitated salt has a porous structure during stage 1. Figure 5 illustrates the SEM images of the precipitated salt at the surface with different magnification factors after 18 h and 1 week. They indicate that the precipitated salt is porous even after 18 hours. At later stages of drying, however, the structure is modified, with the pores being blocked by further salt precipitation. Therefore, during stage 1, the precipitated porous salt may draw the liquid to the surface where evaporation actually occurs, maintaining

the hydraulic connections between the receding front and the evaporation surface, despite the existence of the precipitated salt at the surface [6,7]. As evaporation proceeds, however, further salt precipitation eventually blocks the pores of the efflorescence, resulting in the interruption of capillary flow to the surface.

## IV. SUMMARY AND CONCLUSIONS

In summary, using direct pore-scale imaging, we investigated the 3D dynamics of salt crystallization in drying porous media and delineated the governing mechanisms that affect salt growth and precipitation patterns in saline porous media. Moreover, the SEM imaging confirms unambiguously the porous nature of the precipitated salt, its evolution at the evaporation surface, and its role in maintaining a relatively constant evaporation rate, even when the surface is covered by the precipitated salt.

## ACKNOWLEDGMENTS

We are grateful to Peng Zhou, who conducted the SEM imaging at the Boston University Photonics Center. The x-ray microtomography experiments were performed at the Center for Nanoscale Systems at Harvard University. This work was supported in part by the ACS Petroleum Research Fund (PRF No. 52054-DNI6).

[1] G. W. Scherer, Cem. Concr. Res. **34**, 1613 (2004); R. M. Espinosa Marzal and G. W. Scherer, Environ. Geol. **56**, 605 (2008); M. Schiro, E. Ruiz-Agudo, and C. Rodriguez-Navarro, Phys. Rev. Lett. **109**, 265503 (2012).

[2] U. Nachshon, E. Shahraeeni, D. Or, M. Dragila, and N. Weisbrod, Water Resour. Res. **47**, W12519 (2011); N. Sghaier and M. Prat, Transp. Porous Media **80**, 441 (2009); H. Eloukabia, N. Sghaier, S. Ben Nasrallaha, and M. Prat, Int. J. Heat Mass Transfer **56**, 80 (2013); M. Norouzi Rad and N. Shokri, Geophys. Res. Lett. **39**, L04403 (2012).

[3] S. Veran-Tissoires, M. Marcoux, and M. Prat, Europhys. Lett. **98**, 34005 (2012); Phys. Rev. Lett. **108**, 054502 (2012); H. Eloukabi, N. Sghaier, M. Prat, and S. B. Nassrallah, Chem. Eng. Technol. **34**, 1085 (2011).

[4] C. Cortes and V. Vapnik, Mach. Learn. **20**, 237 (1995); J. C. Platt, in *Advances in Kernel Methods: Support Kernel Machine*, edited by B. Scholkopf, C. Burges, and A. J. Smola (MIT Press, Cambridge, MA, 1999), Chap. 12, p. 185.

[5] N. Shokri, P. Lehmann, and D. Or, Phys. Rev. E **81**, 046308 (2010); N. Shokri and M. Sahimi, *ibid*. **85**, 066312 (2012); N. Shokri, M. Sahimi, and D. Or, Geophys. Res. Lett. **39**, L09401 (2012).

[6] P. Lehmann, S. Assouline, and D. Or, Phys. Rev. E **77**, 056309 (2008); N. Shokri and D. Or, J. Colloid Interface Sci. **391**, 135 (2013); Water Resour. Res. **47**, W09513 (2011); N. Shokri and G. Salvucci, Vadose Zone J. **10**, 1309 (2011).

[7] A. G. Yiotis, A. G. Boudouvis, A. K. Stubos, I. N. Tsimpanogiannis, and Y. C. Yortsos, AIChE J. **50**, 2721 (2004).

[8] S. Chatterji, Cem. Concr. Res. **30**, 669 (2000).

[9] L. Guglielmini, A. Gontcharov, A. J. Aldykiewicz, Jr., and H. A. Stone, Phys. Fluids **20**, 077101 (2008); H. P. Huinink, L. Pel, and M. A. J. Michels, *ibid*. **14**, 1389 (2002).

[10] M. Sahimi, *Flow and Transport in Porous Media and Fractured Rock*, 2nd ed. (Wiley-VCH, Weinheim, Germany, 2011); Rev. Mod. Phys. **65**, 1393 (1993).

[11] X. Y. Liu, J. Chem. Phys. **112**, 9949 (2000).